REVISTA DE LA
ASOCIACIÓN GEOLÓGICA ARGENTINA
www.geologica.org.ar

Volumen 80 (1)

Marzo 2023

# The occurrence of graphite in Campo del Cielo as a clue to understanding the formation scenario of non-magmatic iron meteorites

**Laura Noel GARCÍA[1,2,3], Marcela SAAVEDRA[1,2], Pouyan SHEN[4], María Eugenia VARELA[1,2] y Laura BAQUE[1,5]**

[1]Consejo Nacional de Investigaciones Científicas y Técnicas (CONICET), CABA, Argentina

[2]Instituto de Ciencias Astronómicas, de la Tierra y del Espacio (ICATE), Universidad Nacional de San Juan, CONICET, San Juan, Argentina

[3]Instituto de Mecánica Aplicada (IMA), Universidad Nacional de San Juan, San Juan, Argentina

[4]Department of Materials and Optoelectronic Science, National Sun Yat-sen University, Kaohsiung, Taiwan

[5]Instituto de Nanociencia y Nanotecnología (INN), CNEA-CONICET, Centro Atómico Bariloche (CAB), S.C. de Bariloche, Argentina

E-mail: lngarcia@conicet.gov.ar

**Editor:** Diego A. Kietzmann

Recibido: 20 de enero de 2023

Aceptado: 20 de abril de 2023

## ABSTRACT

The purpose of this research is to assess the carbon vapor deposition scenario as proposed in the literature for graphite formation in non-magmatic iron meteorites. For this aim, graphite occurrence in a sample of the Campo del Cielo Argentinean iron meteorite was explored through optical and electron microscopy, Raman spectroscopy, and time-of-flight secondary ion mass spectrometry. From the results, an alternative setup shall be considered for graphite formation, which would provide evidence for understanding the formation of non-magmatic meteorites, still under discussion.

**Keywords:** Argentinian meteorites, Iron meteorites, Carbon Vapor Deposition, Raman spectroscopy, ToF-SIMS.

## RESUMEN

*La ocurrencia de grafito en Campo del Cielo como pista para entender el escenario de formación de los meteoritos de hierro no magmáticos.*

El propósito de esta investigación es el de evaluar el escenario de deposición de carbono por vaporización propuesto en la literatura para explicar la formación de grafito en los meteoritos de hierro no magmáticos. Para ello, se exploraron las ocurrencias de grafito en una muestra del meteorito argentino Campo del Cielo a través de microscopía óptica y electrónica, espectroscopía Raman, y espectrometría de masas de iones secundarios detectados por tiempo de vuelo. De los resultados de este trabajo se desprende que deberían considerarse escenarios alternativos de formación de grafito, los cuales podrían proveer evidencia para entender la formación de los meteoritos no magmáticos, aún bajo discusión.

**Palabras clave:** meteoritos argentinos, meteoritos de hierro, deposición de carbono por vaporización, espectroscopía Raman, ToF-SIMS.

## INTRODUCTION

Iron meteorites provide valuable information about the early history of the Solar System, which is related to the igneous and impact processes that shaped the first planetesimals (e.g. Scott et al. 2020). These represent only 5.7% of the total falls and are mostly conceived as products of a differentiation process inside planetesimals (e.g. Scott and Wasson 1975), following the conventional formation model, which implies its

development from a single metallic melt or core (e.g. Goldstein et al. 2009). In contrast to these magmatic meteorites, non-magmatic meteorites represent approximately 15% of iron meteorites and present chemical characteristics that are not in line with a differentiation process (Wasson and Kallemeyn 2002, Worsham et al. 2016). These meteorites are graphite rich and much richer in silicates (Benedix et al. 2000, Ruzicka 2014), and include the group of meteorites designated as IAB irons, mainly formed by a metallic Fe-Ni matrix with a Ni content of 6.5-7.5 wt-%. Silicates are mainly of chondritic composition (i.e., undifferentiated material) and are associated with troilite-graphite inclusions, distributed throughout the metallic mass. At this point, a question naturally arises: how is it possible that a pristine material is included in the metal if the metal itself represents the product of primitive material differentiation? One possible scenario could account for both phases being in a liquid state by the time of their encounter; however, the immiscible liquid made up of metal and silicates should separate gravitationally, even under zero gravity conditions, due to the enormous surface tension of the metallic liquid. In an alternative setup, an impact event between melted metal and a fragmented rock, would result in the intimate association of metal and silicates (Benedix et al. 2000, Ruzicka 2014); yet, how could it be possible that the temperature experienced in this type of collisions was high enough to melt the metal, but not to affect the chondritic composition of the silicate inclusions? Despite the large number of models that have been developed to explain the petrography of non-magmatic meteorites (Goldstein et al. 2021 and references therein), there is still not a comprehensive and satisfactory proposal.

Although most of the aforementioned models require high temperature, Maruoka et al. (2003) suggested a low-temperature origin of IAB iron meteorites after the analysis of carbon isotopic compositions of graphite in San Juan (a Campo del Cielo mass according to Saavedra et al. 2022). The authors reported carbon isotopic heterogeneities on graphite located inside silicate inclusions, between the inclusions and the metal, and inside the metal. Preservation of such isotopic heterogeneities would require low-temperature processes; therefore, they concluded that the graphite inclusions never experienced high-temperature events. They suggested the decomposition of carbonyls as involved in the formation of metal and graphite in the San Juan mass, as previously proposed by Kurat et al. (2000) for Canyon Diablo (IA) graphite-metal meteorite. The reaction would be accounted for by the decomposition of the carbonyl and formation of metal: $Fe(CO)_5 \rightarrow Fe^0 + 5CO$, followed by the formation of carbon: $2CO \rightarrow C + CO_2$, which would be accompanied by isotopic fractioning of carbon isotopes between graphite and carbon dioxide. This would be achieved by a chemical vapor deposition (CVD) process. In this work, graphite as present in a Campo del Cielo sample (Argentinian IAB iron), is investigated employing Raman microspectroscopy and ToF-SIMS to evaluate this proposed CVD scenario that would help to constrain the origin of IAB iron meteorites.

Finally, it should be noted that the IAB group is one of the many groups that have been proposed as possible analogous meteorites to the Psyche asteroid, a target of the NASA Psyche mission that will launch in 2023 (Elkins-Tanton et al. 2020). Psyche would be a mixture of silicates with low FeO content and 30-60 v/v% of metal. The IAB group would be an especially attractive candidate considering that many of the meteorites grouped under this classification contain silicates with low FeO content, and their occurrence (the second largest group of metallic meteorites), suggests a possible relationship with the massive M-type asteroids, including Psyche. Previous observations suggest that large variations in metal abundances exist on the Psyche surface, which would favor a scenario of intimate mixing between silicates and metal, as should occur in the parent body of the IAB iron meteorites. Therefore, the advances achieved in the understanding of the origin of the IAB meteorites may be complemented (or opposed) with those of the Psyche mission.

## SAMPLE AND METHODOLOGY

### Optical and scanning electron microscopy

One Campo del Cielo sample (IAB iron coarse octahedrite, Buchwald 1975), was the focus of the present study. The original sample as a whole is presented in Fig. 1, half of which is available at the ICATE repository. Optical microscopy (OM) under reflective light and a ZEISS Scanning Electron Microscope (SEM) EVO MA 10W equipped with an EDS (energy-dispersive X-ray spectroscopy) detector, were used for the aim of describing the petrography of the sample and registering graphite occurrences. From SEM inspection, both secondary electron and backscattered electron images (SEI and BEI, respectively) were recorded. For this purpose, the sample was polished by conventional procedure, including diamond paste polishing. Carbon coating was necessary for SEI and BEI acquisition.

### Raman microspectroscopy

Before conducting the OM/SEM, Raman microspectroscopy was employed to assess carbon organization at the atomic scale in different graphite occurrences. Reference graphite is characterized by an individual band at 1584 $cm^{-1}$ which is referred to as the ‘G band’ (e.g. Pimenta et al. 2007). As the

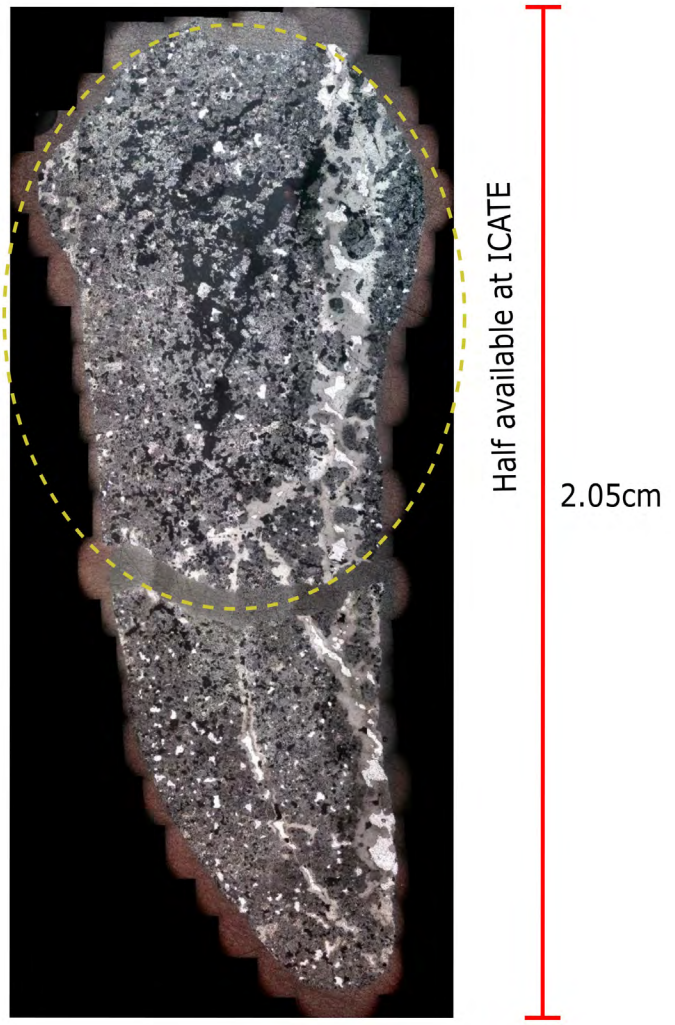


**Figure 1.** Optical-microscope panoramic view of the Campo del Cielo meteorite sample.

structural disorder increases, carbons show additional bands known as 'defect bands', the strongest being the 'D band', centered at ~1350 $cm^{-1}$ (Fig. 2). Their intensity increases as a function of the amount of disorder, together with broader D and G bandwidths.

At this step, the sample had neither been coated (20 nm-thick amorphous carbon coating could bias Raman spectra by broadening the bands) nor been prepared by polishing with water or diamond paste (only coarse polishing with emery paper) as a structural disorder is introduced in polished sections. Nevertheless, as polishing artifacts could still have been present, their effects were reviewed in the literature. In this regard, Ammar et al. (2011, 2012) examined how to extract the structural information from Raman data modified by the effect of polishing. They found that both the D-band intensity and the ratio of the D and G-bands intensities ($I_D/I_G$), rise with polishing, whereas the Full Width at Half Maximum of the G band ($FWHM_G$) remains fairly constant. The authors also proposed the following function for evaluating the intensity ratio: $FWHM_G$=14+35 $I_D/I_G$ ($R^2$=0.99) [Equation I], from which $I_D/I_G$ can be estimated.

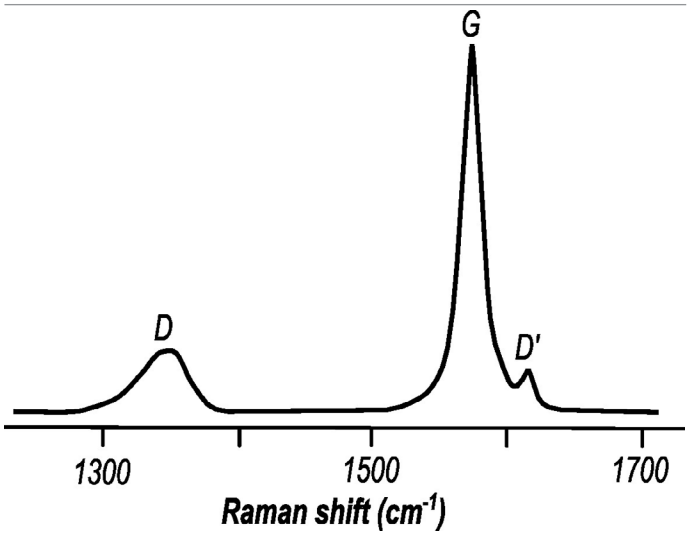


**Figure 2.** Typical Raman bands of graphite in the first-order region.

Punctual spectrums paths were acquired with a separation of ~ 5 µm (minimum manual step) in a Confocal Horiba Jobin-Yvon LabRam HR. The acquisition setup was 0.33 mW with a 100x objective and an incident beam with a 514.5 nm wavelength. Each spectrum is the average of 10 spectrums of 10 s of collecting time. Raman shift values were registered from 200 to 1700 $cm^{-1}$. A spatial resolution of 1.5 $cm^{-1}$ is expected. No damage was observed in the sample associated with the light intensity absorbed by it.

For processing the individual spectrum, the Spectragryph software was employed (https://www.effemm2.de/spectragryph/about.html). Noisy spectra were discarded, and individ-

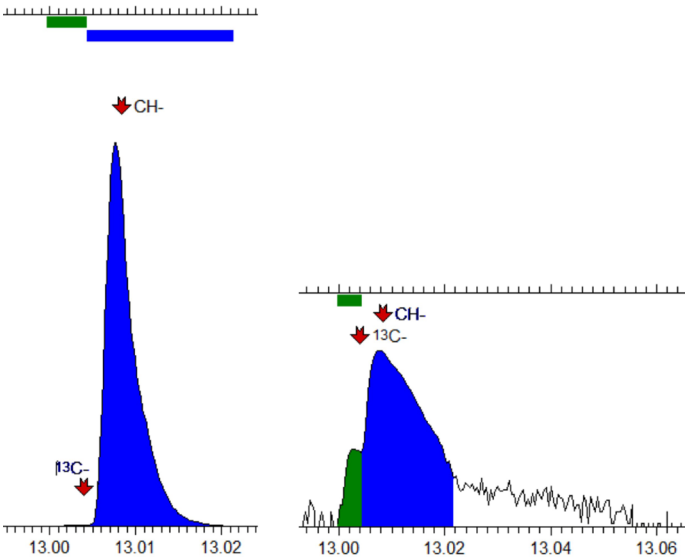


**Figure 3.** Position of $^{12}C^{1}H^{-}$-signal and $^{13}C^{-}$ peak in linear and logarithmic scale

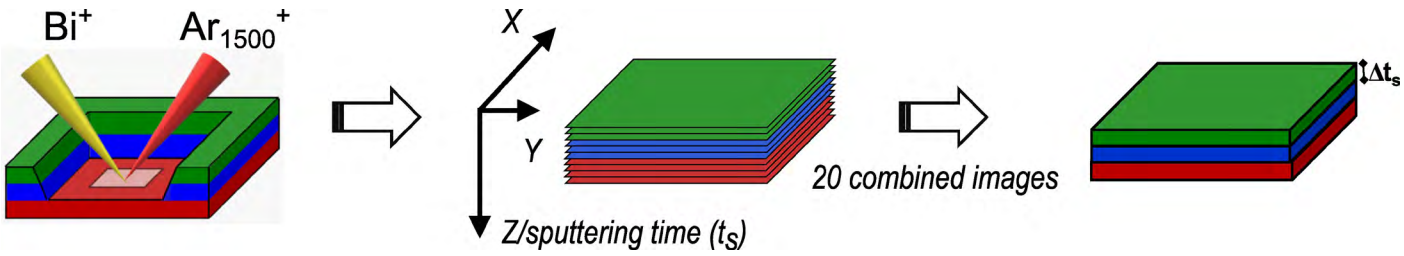


**Figure 4.** Representation of the process for obtaining information on the graphite formation. $\Delta t_s$ represents the sputtering time of $Bi^+$ with in-situ surface cleaning by $Ar_{1494}^+$.

ual polynomial baselines were generated and subtracted. The $FWHM_G$ at each position was obtained after normalization, which was performed by setting each spectrum's highest peak within a visible area to the value of 1.

### Time-of-Flight Secondary Ion Mass Spectrometry

In order to evaluate previous results concerning carbon isotope heterogeneity (e.g. Maruoka et al. 2003), *time-of-flight* (ToF-) secondary ion mass spectrometry (SIMS) was utilized. This technique has been recently introduced for extraterrestrial sample analysis (Stephan, 2001 and references therein) and can detect elemental and molecular information from the outermost sample surface with a low primary ion beam dose ($1\times10^{12}$ atoms/cm$^2$ or less). This is also named static SIMS mode because of the negligible sputtering (<0.1% of a monolayer) during data acquisition, which preserves the sample, unlike traditional SIMS. Besides, in ToF-SIMS, all the secondary ion species either with positive or negative polarity, are detected at the same time.

Carbon forms both positive and negative secondary ions during sputtering, depending on the chemical environment (Stephan, 2001): hydrocarbons generate $C^+$ and $C^-$ secondary ions, whereas carbonates and carbides mainly form $C^-$ ions; CH, $CH_2$, and $CH_3$ are also observed in both polarities. Therefore, for the measurement of $^{12}C/^{13}C$, the $^{12}C^1H$-signal and the $^{13}C$ peak (Fig. 3) have to be separated.

On this occasion, the acquisition process was archived through a Time-of-flight Secondary Ion Mass Spectrometer TOF.SIMS 5-100, IONTOF GmbH Germany installed at GIA-CNEA, Argentina. As contamination usually is a severe problem in ToF-SIMS measurements, the surface was cleaned in situ by depth profiling for 0.125 s. A depth profile was acquired in spectrometry mode from a graphite formation by using Bi+ as the analysis beam with 30 keV energy and 0.5 pA current and $Ar_{1494}$+ clusters as the sputtering beam with 10 keV and 13.3/4 nA. The total sputtered area was 750 x 750 µm$^2$ and the analysis area was 500 x 500 µm$^2$ with a resolution of 128 x 128 pix. The depth profile was performed in non-interlaced mode using a 21 V electron beam for charge compensation. The acquisition process is represented in Fig. 4.

## RESULTS

### Petrography

The silicate inclusion has an elongated shape with a coarse-grained texture with grain sizes typically ≥100 µm across that varies from place to place. This inclusion is composed mainly of olivine, pyroxene, and plagioclase with variable amounts of troilite, metal, apatite, and a graphite/metal

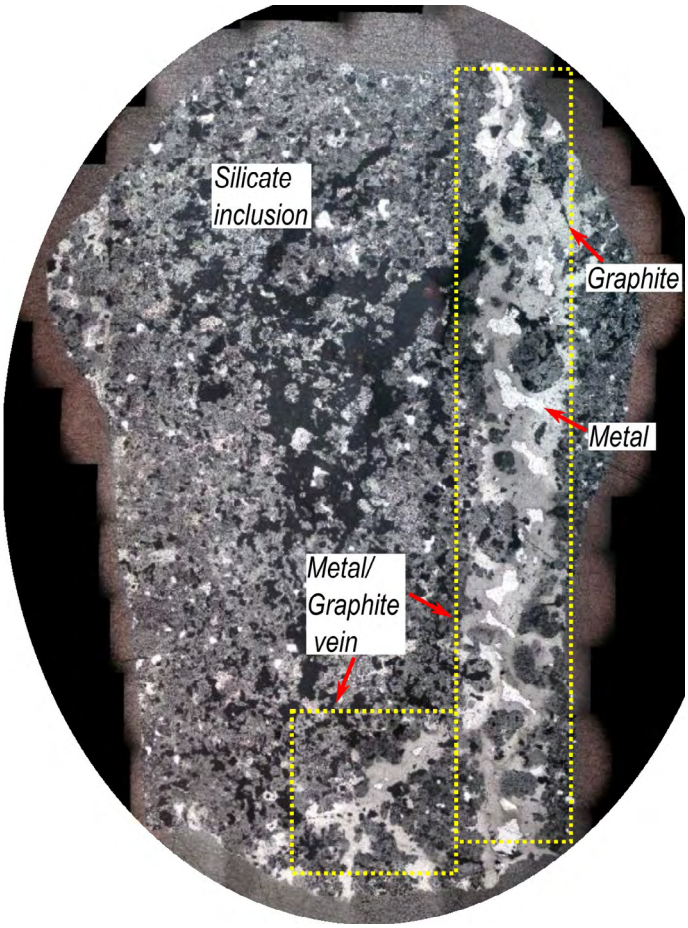


**Figure 5.** Optical-microscope panoramic view of the sample where the main regions with metal, graphite, and silicate veins are recognized.

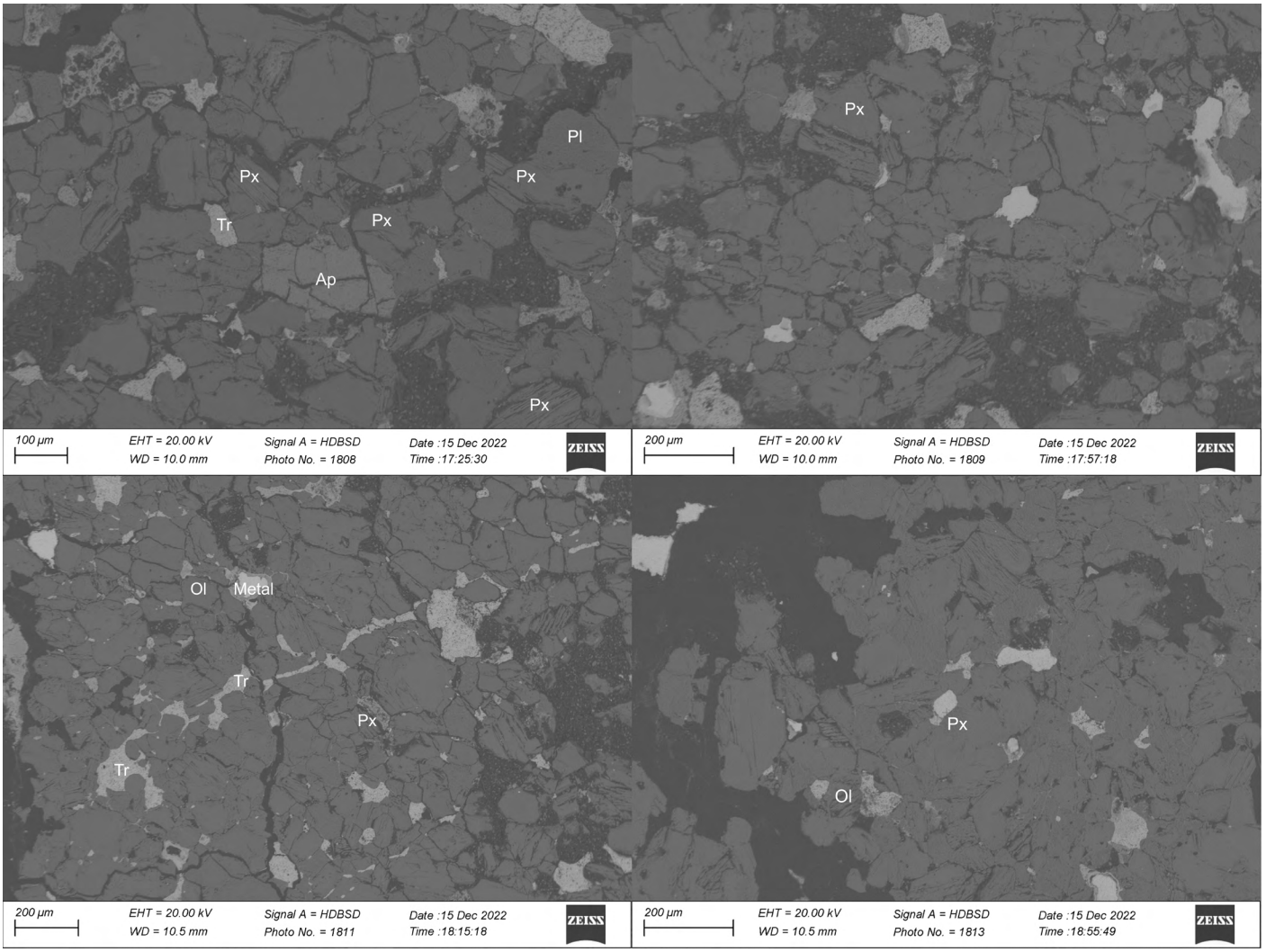


**Figure 6.** BEI of main phases as present in the sample under study: plagioclase (Pl), pyroxene (Px), apatite (Ap), troilite (Tr), olivine (Ol), metal.

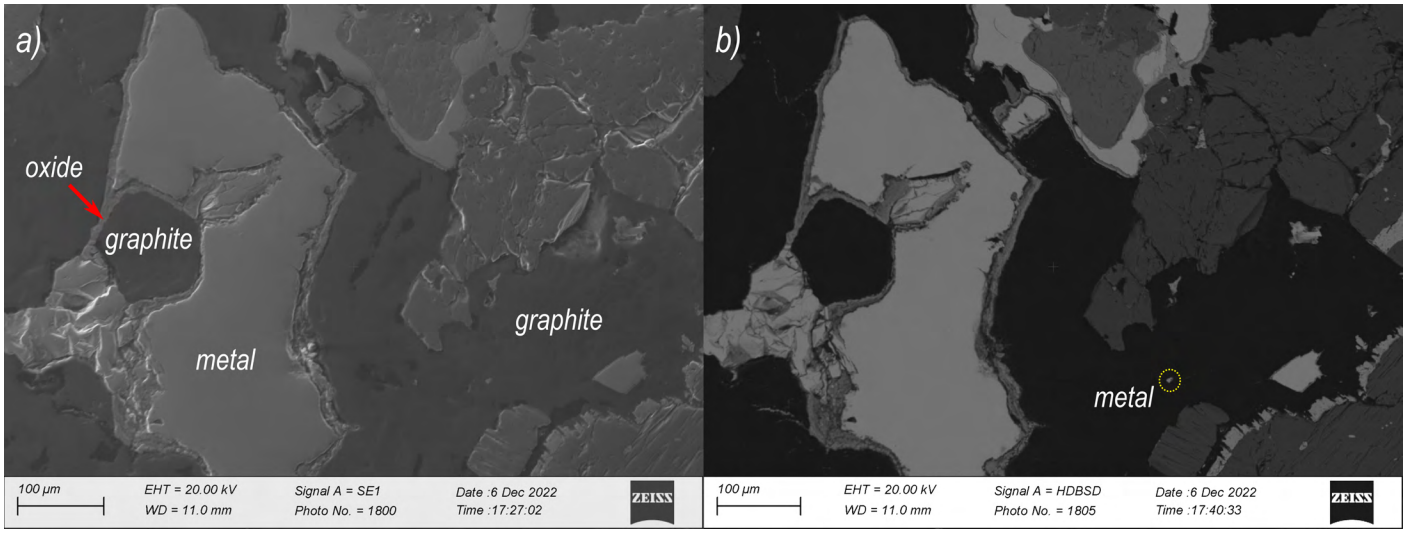


**Figure 7.** a) SEI and b) BEI showing an euhedral graphite grain isolated in the metallic phase and graphite as dense aggregates with a tramp metal inclusion (circled) and surrounded by the metal and silicate grains.

vein (Fig. 5). The vein is composed of metal, graphite, and silicate and occurs along pre-existing fractures that run across the inclusion.

From BEI in Fig. 6, the pyroxene crystals (Op x= En90.56,

Fs6.95, Wo1.65; Cpx = En49.49, Fs3.18, Wo45.08) vary in shape from anhedral to subhedral (tabular) with laths up to 200 µm long. No reaction rims or exsolution lamellae were observed. Plagioclase crystals (An16.45) occur with irregular shapes (≥100 µm) with rounded grain boundaries. Olivine (Fo94.34) appears as crystals of sizes greater than 100 µm in apparent diameter with irregular shapes. The surface shows few secondary fractures. Apatite frequently appears as highly fractured, randomly oriented, subhedral-anhedral crystals with sizes more than 200 µm in length. It develops concave boundaries in contact with silicate crystals. The troilite and metal have a random distribution in the silicate inclusion. The boundaries between this phase with the host (pyroxenes, olivines, and plagioclases) are sharp up to more than 100 µm in size with irregular shapes. The representative chemical compositions of silicates in Campo del Cielo are available in Table I (supplementary material).

Besides, graphite is present throughout the graphite/metal vein (Fig. 5), as isolated bodies immersed in the metal (usually surrounded by an oxide layer as in Fig. 7), and as dense aggregates in the metal vein (Fig. 7 and Fig. 8). According to EDS analysis, Ni content in the metallic phase is lower than 5 wt-% which is consistent with Ni content as expected in kamacite, a Fe-Ni alloy (bcc-α). In Fig. 7 and Fig. 8, the presence of isolated kamacite in the graphite aggregates was identified by combining BSI and EDS analyses. No other inclusions or species were detected, which is in line with Raman's results, as follows.

### Raman measurements

The paths analyzed in the chosen graphite formations for Raman measurements are indicated as arrows in Fig. 9, whereas the spectra recorded for Path A are displayed in Fig. 10 as an example. After determining $FWHM_G$ in each position by Equation I, $I_D/I_G$ was estimated as $I_D$ was present in the spectrograms. From Fig. 11 it can be inferred that $I_D/I_G$ randomly variates from the center to the periphery of the graphite occurrences with no clear tendency, i.e., there is an unsystematic variation in graphite disorder throughout aggregates with grain boundaries and across graphitic particles with turbostratic graphite layers stacking/spreading outwards from a nucleus as spherulite after a solidification process (Garcia et al. 2023). In turbostratic graphite, graphite layers possess no periodicity; instead, they are misaligned with each other by random translation and rotation, and the interlayer spacing varies from plane to plane.

### Time-of-Flight Secondary Ion Mass Spectrometry

Finally, the distribution of carbon species was recorded for Path D in Fig. 9. The results for different sputtering times are available in Fig. 12. After 125 s, the surface cleaning process was completed and the significant deprotonation at the center of the graphite formation to shape the H-depleted center and H-rich periphery was evidenced. On the other hand, $^{12}C$ and $^{13}C$ irregular dispersion did not significantly change upon the sputtering time increase.

## DISCUSSION

Raman spectroscopy has been widely used for the characterization of graphene layers (a single layer of carbon atoms organized as a two-dimensional honeycomb lattice na-

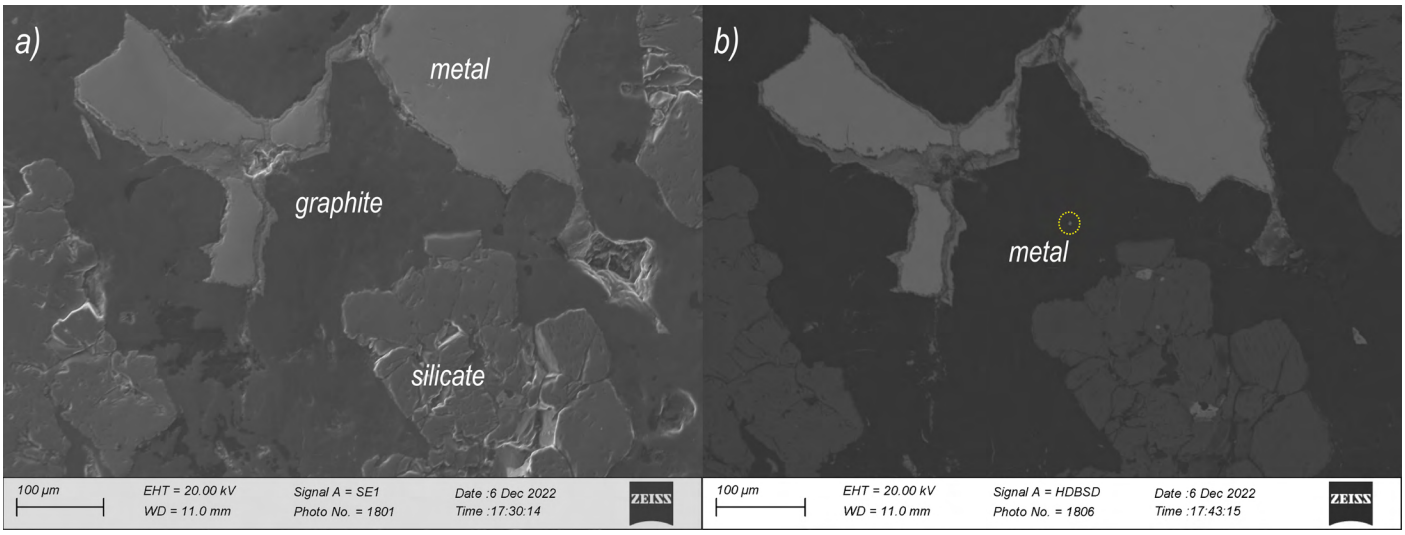


**Figure 8.** a) SEI and b) BEI of another area showing also graphite as dense aggregates with tramp metal inclusion (circled) and surrounded by the metal and the silicate grains.

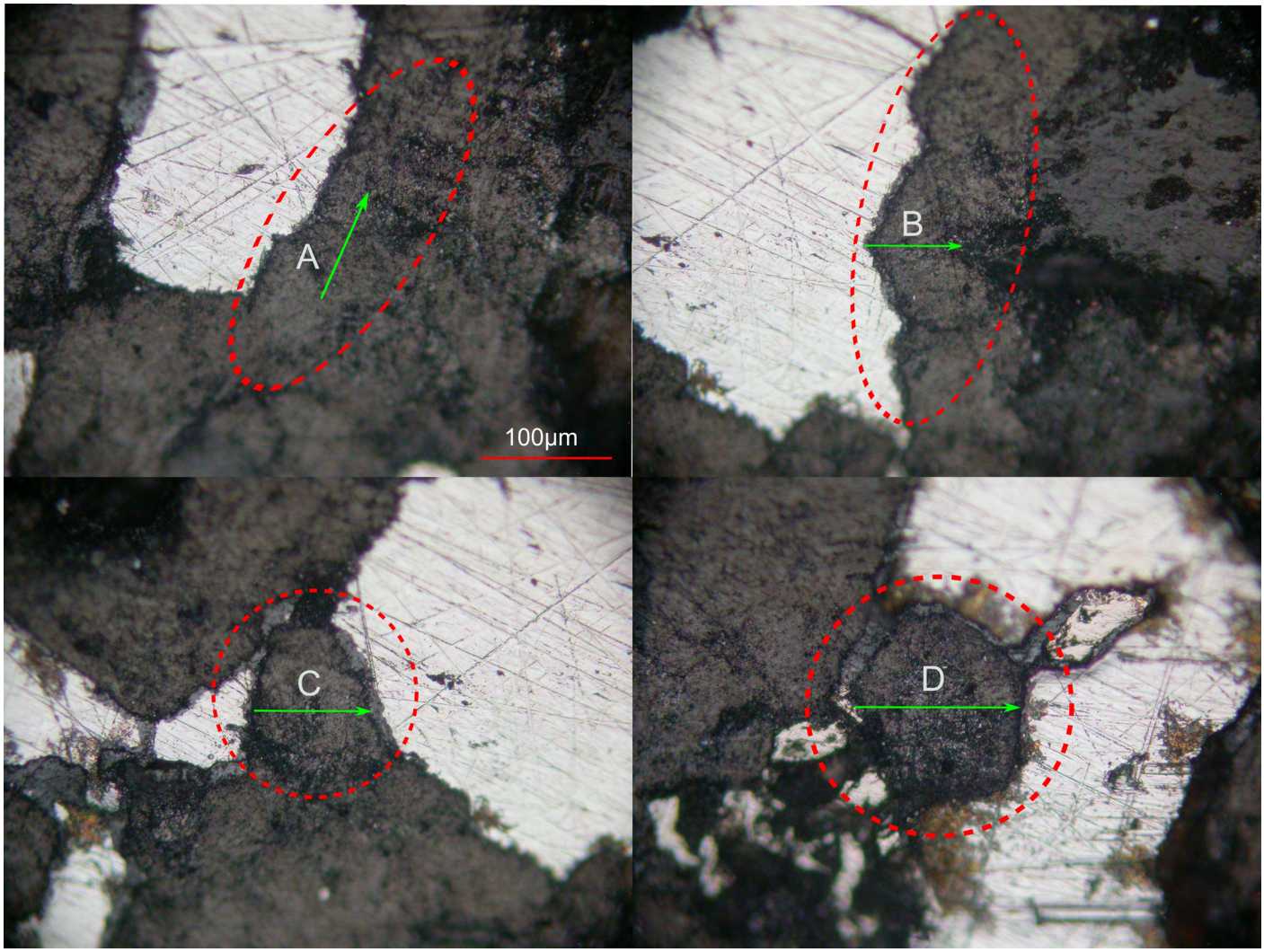


**Figure 9.** Variants of graphite occurrences: A and B paths in aggregates; C and D in partially isolated subhedral and euhedral grains surrounded by the metal. The paths followed during Raman studies are indicated by arrows.

nostructure) as obtained from CVD. For instance, Naghdi et al. (2016), characterized graphene as obtained by CVD on a molybdenum foil at different growth temperatures by Raman spectrometry. They found the lowest $I_D/I_G$ values for graphene layers obtained at 1000 °C (in contrast to 1100 and 1200 °C), suggesting that graphene defects decreased at the higher temperature. Then, $I_D/I_G$ is a temperature-dependent parameter in graphene/graphite formation besides crystalline-size dependence. In this context, the randomly distributed $I_D/I_G$ ratio along the paths measured by Raman spectroscopy (Fig. 11) could be the consequence of variations in the temperature process (different depositions steps) and crystalline size. When combined with the textural observations, graphite in this Campo del Cielo sample could barely be related to a CVD process as it would result in the formation of widespread graphene layers on the metal/silicate grains/particles like that overlain on a substrate (the reader might check the overview in Saeed et al. 2020) or nanotubes (graphene sheets rolled into a tube) and other graphene variants after Ni (Kukovitsky et al. 2000) or Fe-Ni (Samaniego et al. 2015) alloys. Noteworthy is the recent publication by Begunova et al. (2019, 2020) who synthesized carbon nanotubes on two different meteorites: Chinga ataxite and the metallic phase of Seymchan, a pallasite. Such hollow carbon forms are drastically different from the C-rich fluid-infiltration solidified vein (Fig. 5) or the isolated/aggregated graphite formations (Fig. 7 and Fig. 8). Besides, graphite selective protonation, as manifested by the ToF-SIMS measurements of hydrocarbon species from a representative graphitic particle showing progressive deprotonation at its center upon $Ar_{1494}^+$ beam sputtering (Fig. 12), could be related to the infiltration of a C-H rich fluid, having little or no relation to the alleged CVD process.

As hypothesized by Maruoka et al. (2003), carbonyl decomposition through a CVD process could explain the carbon isotope heterogeneity as presented in Fig. 12. Nevertheless, experimentally, there is always an alternative mechanism for

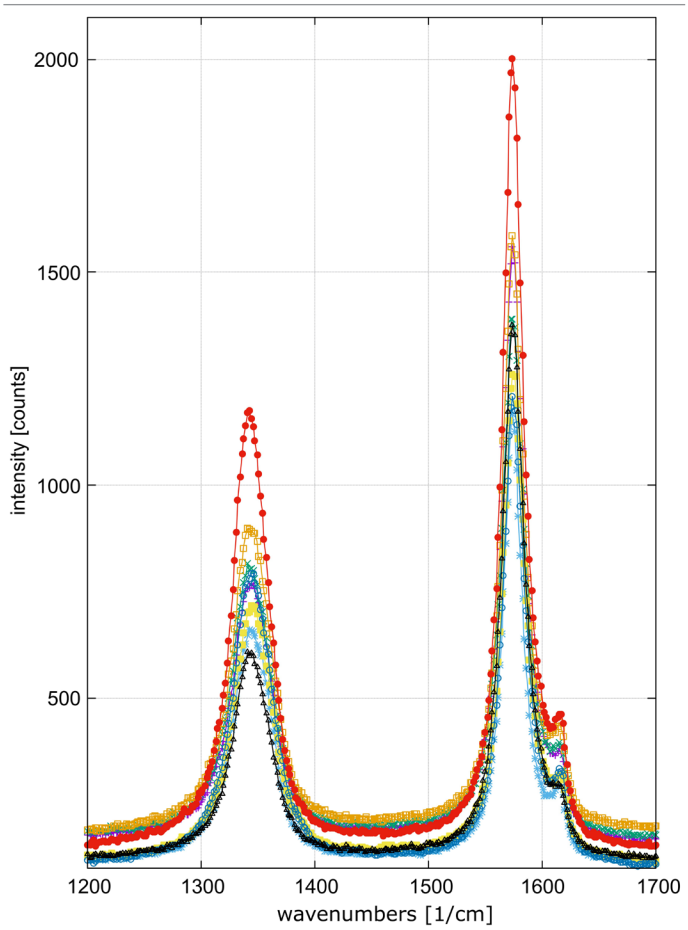


**Figure 10.** Spectra of each position of Path A in figure 9.

the formation of graphite aggregates with special external morphology (Fig. 7 and Fig. 8), such as solidification, solid-state formation, shock compression, etc., as evidenced by numerous experiments on C-bearing materials. Furthermore, the diversified temperature-pressure-composition (T-P-C) conditions among different specimens and within them, cannot be disregarded for explaining the different graphite occurrences. In this connection, Korsakov et al. (2019) characterized natural graphite cuboids from a series of terrestrial complexes, all of which were polycrystalline aggregates composed either of small graphite cuboids or graphite flakes. Based on their stability fields, the authors concluded that the cuboids would occur in a wide range of T-P conditions by graphite precipitation from fluid/melt. Thus, an ideal master scenario for the formation mechanism of graphite in non-magmatic meteorites by carbon vapor deposition may fail to explain the overall diversified textures due to complicated T-P-C paths as a function of time and space from macro to the nanoscale of meteorites. Still, physical-chemical proposals are useful to give a reasonable interpretation for the individual graphite occurrences in each meteorite, though exclusive, not inclusive. In fact, a high-temperature solidification scenario may also account for graphite formation in non-magmatic irons, as supported by nanostructure characterization of one isolated graphite formation in another Campo del Cielo sample in a recent investigation by Garcia et al. (2023).

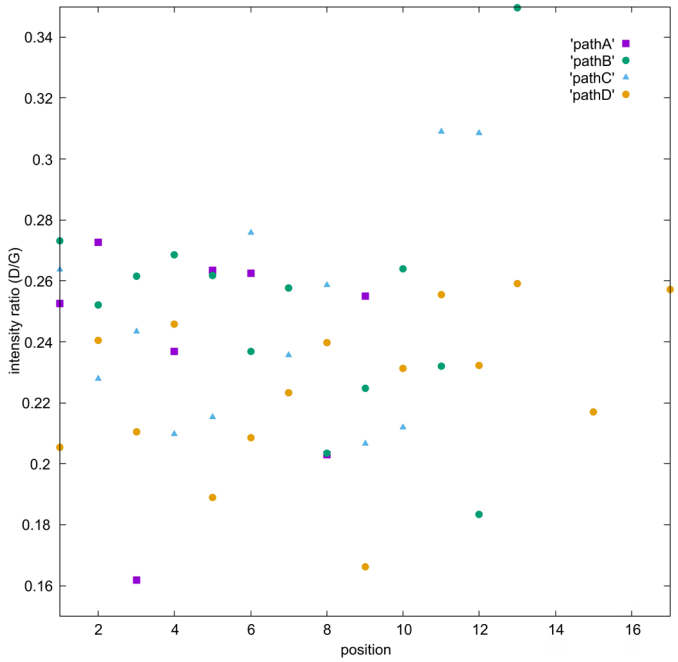


**Figure 11.** Estimated $I_D/I_G$ ratio for each of the paths in figure 9. The position represents the collected punctual spectra which are separated by ~ 5 µm.

## CONCLUSIONS

A carbon vapor deposition mechanism has been previously proposed as responsible for explaining the isotopic carbon heterogeneities found in graphite of non-magmatic iron meteorites, which would relate their origin to low-temperature processes. However, the origin of non-magmatic iron meteorites is still a matter of debate. In this work, this proposal was assessed by a combination of optical and scanning electron microscopy, together with Raman spectroscopy and time-of-flight secondary ion mass spectrometry focused on graphite formations in a Campo del Cielo sample (IAB iron, non-magmatic). The results did not validate carbonyl decomposition through a carbon vapor deposition scenario. This is in line with newly available results for graphite formation in IAB irons, which suggest it would be the result of a solidification process. Consequently, alternative scenarios shall be considered in the formation of these meteorites, which will be explored in future work.

## ACKNOWLEDGMENTS

The authors are grateful for the financial support of the

CONICET and of the Agencia I+D+I (PICT #1562) and acknowledge to LANN-SNM laboratory at INFICQ for assistance in Raman measurements.

**Supplementary material:** https://revista.geologica.org.ar/raga/article/view/1685/1653

## REFERENCES

Ammar, M.R., Charon, E., Rouzaud, J.N., Aléon, J., Guimbretière, G., and Simon, P. 2011. On a Reliable Structural Characterization of Polished Carbons in Meteorites by Raman Microspectroscopy. Spectroscopy Letters 44: 535-538.

Ammar, M.R., and Rouzaud, J.N. 2012. How to obtain reliable structural characterization of polished graphitized carbons by Raman microspectrometry. Journal of Raman Spectroscopy 43: 207-211.

Benedix, G.K., McCoy, T.J., Keil, K., and Love, S.G. 2000. A petrologic study of the IAB iron meteorites: constraints on the formation of the IAB-winonaite parent body. Meteoritics & Planetary Science 35: 1127-1141.

Begunova, A., Yakovlev, G., Kamalov, R., Pankrushina, E., and Grokhovsky, V. 2019. Influence of Seymchan meteorite structure on the synthesis of carbon nanotubes. AIP Conference Proceedings 2174.

Begunova A., Yakovlev G., Grokhovsky V., Kamalov R., and Pankrushina E. 2020. Synthesis of nanostructures on the Chinga meteorite. AIP Conference Proceedings 2313.

Buchwald, V. 1975. Handbook of iron meteorites. Their history, distribution, composition and structure. Vol. 1: Iron meteorites in general. University California Press, 1426 p., Berkeley.

Elkins-Tanton, L.T., Asphaug, E., Bell, J.F., Bercovici, H., Bills, B., and Binzel, R. et al. 2020. Observations, meteorites, and models: a preflight assessment of the composition and formation of (16) Psyche. Journal of Geophysical Research: Planets 125: e2019JE006296.

García, L.N., Shen, P., Quirico, E., Varela, M.E., Montagnac, G., Tolley, A., Stefanescu, D., and Baruj, A. 2023. On the occurrences and formation mechanisms of cliftonites: the case of Campo del Cielo iron meteorite. Carbon 208: 60-71. Goldstein, J.I., Scott, E.R.D, and Chabot, N.L. 2009. Iron meteorites: crystallization, thermal history, parent bodies, and origin. Chemie der Erde 69: 293-325.

Goldstein, J., Scott, E., Winfield, T., Yang, J., and Rubin, A. 2021. Cooling rates and impact histories of group IAB and other IAB complex iron meteorites inferred from zoned taenite and the cloudy zone. Meteoritics & Planetary Science 57.

Korsakov, A., Rezvukhina, O., Jaszczak, J., Rezvukhin, D., and Mikhailenko, D. 2019. Natural graphite cuboids. Minerals 9(2): 110.

Kukovitsky, E.F., L'vov, S.G., and Sainov, N.A. 2000. VLS-growth of carbon nanotubes from the vapor. Chemical Physics Letters 317: 65-70.

Kurat, G., Sylvester, P., Kong, P., and Brandstätter, F. 2000. Heterogenous and Fractionated Metal in Canyon Diablo (IA) Graphite-Metal Rock. Lunar and Planetary Science Conference XXXI: 1666.

Maruoka, T., Kurat, G., Zinner, E., Varela, M.E., and Ametrano, S. 2003. Carbon isotopic heterogeneity of graphite in the San Juan mass of the Campo del Cielo IAB iron meteorite. Lunar and Planetary Science Conference XXXIV: 1663.

Naghdi, S., Rhee, K., Kim, M., Jaleh, B., Park, S-J. 2016. Atmospheric chemical vapor deposition of graphene on molybdenum foil at different growth temperatures. Carbon letters 18: 37-42.

Pimenta, M.A., Dresselhaus, G., Dresselhaus, M.S., Cancado, L.G., Jorio, A., and Saito, R. 2007. Studying Disorder in Graphite-Based Systems by Raman Spectroscopy. Physical Chemistry Chemical Physics 9: 1276-1291.

Ruzicka, A. 2014. Silicate-bearing iron meteorites and their implications for the evolution of asteroidal parent bodies. Chemie der Erde 74: 3-48.

Saavedra, M. E., and Varela, M. E. 2022. 'San Juan', a new mass of the Campo del Cielo meteorite shower. Revista De La Asociación Geológica Argentina 79(1): 168-175.

Saeed, M., Alshammari, Y., Majeed, S., and Alnasrallah, E. 2020. Chemical Vapour Deposition of Graphene—Synthesis, Characterisation, and Applications: A Review. Molecules 25: 3856.

Samaniego J.E., Perez J.F., Solorza O., Garcia A. 2015. Al2O3 + FeCo and Al2O3 + FeNi coatings for multiwalled carbon nanotubes growth. Diamond and Related Materials 53: 18-22.

Scott E. 2020. Iron meteorites: composition, age, and origin. Oxford research encyclopedia of planetary science. Oxford: Oxford University Press.

Scott, E., and Wasson, J.T. 1975. Classification and properties of iron meteorites, Geophys. Reviews of Geophysics 13: 527-546.

Stephan, T. 2001. TOF-SIMS in cosmochemistry. Planetary and Space Science 49:859-906.

Wasson, J.T., and Kallemeyn, G.W. 2002. The IAB iron meteorite complex: a group, five subgroups, numerous grouplets, closely related, mainly formed by crystal segregation in rapidly cooling melts. Geochimica et Cosmochimica Acta 66: 2445-2473.

Worsham, E.A., Bermingham, K.R., Walker, R.J. 2016. Siderophile element systematics of IAB complex iron meteorites: new insights into the formation of an enigmatic group. Geochimica et Cosmochimica Acta 188: 261-283.